Journal of Materials Chemistry C

Accepted Manuscript

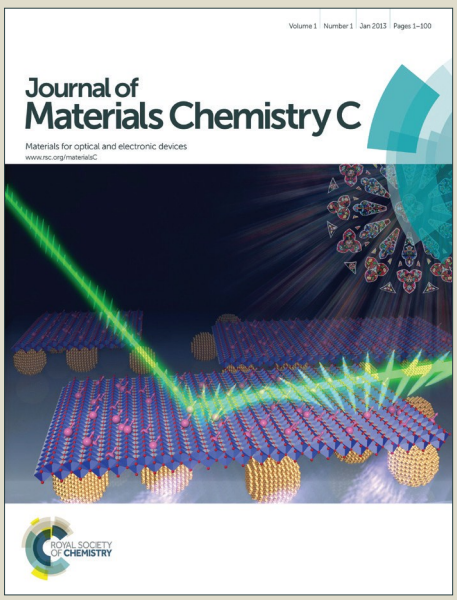

This is an *Accepted Manuscript*, which has been through the Royal Society of Chemistry peer review process and has been accepted for publication.

Accepted Manuscripts are published online shortly after acceptance, before technical editing, formatting and proof reading. Using this free service, authors can make their results available to the community, in citable form, before we publish the edited article. We will replace this *Accepted Manuscript* with the edited and formatted *Advance Article* as soon as it is available.

You can find more information about *Accepted Manuscripts* in the Information for Authors.

Please note that technical editing may introduce minor changes to the text and/or graphics, which may alter content. The journal's standard Terms & Conditions and the Ethical guidelines still apply. In no event shall the Royal Society of Chemistry be held responsible for any errors or omissions in this *Accepted Manuscript* or any consequences arising from the use of any information it contains.

ROYAL SOCIETY OF CHEMISTRY

www.rsc.org/materialsC

Anisotropic Thermally Conductive Flexible Films based on Nanofibrillated Cellulose and Aligned Graphene Nanosheets

Na Song[‡*], Dejin Jiao[‡], Peng Ding[*], Siqi Cui, Shengfu Tang, Liyi Shi

Research Center of Nanoscience and Nanotechnology, Shanghai University, 99 Shangda Road, Shanghai 200444, P.R. China

Abstract: The anisotropic thermally conductive flexible films with nanofibrillated cellulose (NFC) and in situ reduced graphene oxide (RGO) nanosheets are prepared via a vacuum-assisted self-assembly technique. The hybrid films exhibit superior in-plane thermal conductivities, and a value of 6.168 $W•m^{-1}•K^{-1}$ is achieved with 30 wt% GO loading. Noteworthy, the through-plane thermal conductivities are extremely low (≤ 0.072 $W•m^{-1}•K^{-1}$). The high anisotropy of the thermal conductivity is systematically investigated, and correlated to the aligment of RGO nanosheets. Moreover, hybrid films exhibit excellent flexibility as well as high tensile strength. The aligned RGO nanosheets significantly delayed the thermal degradation of the hybrid films. The strongly anisotropic thermally conductive properties of these films can be useful for applications in thermal management.

Keywords: reduced graphene oxide, nanofibrillated cellulose, thermal conductivity, layered structure, anisotropic properties

*Corresponding authors: FAX: +86 21 66134726. E-mail address: snlxf@shu.edu.cn (Na Song), dingpeng@shu.edu.cn (Peng Ding)

Journal of Materials Chemistry C Accepted Manuscript

Graphical abstract:

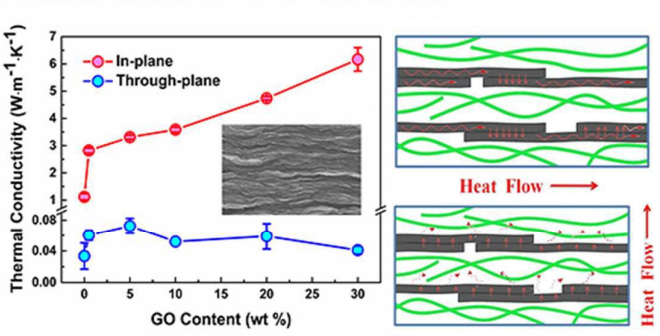

The prepared flexible nanofibrillated cellulose/graphene nanosheets hybrid films possessed significantly anisotropic thermal conductivities. The anisotropy originated from the alignment of graphene nanosheets, which can leads to different thermal resistances along the in-plane and through-plane directions.

Journal of Materials Chemistry C Accepted Manuscript

Introduction

Graphene, a monolayer of hexagonally arranged sp^2-bonded carbon atoms, has elicited substantial interest in the field of efficient thermally management materials because of its extreme in-plane thermal conductivity (approximately 5300 $W \bullet m^{-1} \bullet K^{-1}$).[1-3] Graphene and graphene derivatives have been incorporated into many different polymers to improve the thermal conductivity of composites. For example, 10 vol% of reduced graphene oxide (RGO) and 1 wt% of silica-covered thermally reduced graphene oxide (TRGO) have enhanced the thermal conductivities of polystyrene (PS) and epoxy by approximately 90% and 61%, respectively.[4, 5] Although many improvements have been achieved, the thermal conductivities of composites remain far from the inherent properties of graphene. This problem generally results from the poor dispersion, the discontinuous matrix/filler interfaces and the lack of efficient thermally conductive paths.

To fully exploit the potential of graphene as a superior thermally conductive filler, efforts have been devoted to solving the problems mentioned above, including the alignment of graphene in matrixes,[6, 7] the homogeneous dispersion,[8, 9] and the improvement of the interfacial interaction between graphene and matrixes.[10, 11] Among them, the alignment of graphene is recognized as an efficient method to favor the formation of consecutive thermally conductive paths, along which the thermally contact resistance is minimized.[12] Generally, aligned fillers often impart composites with markedly different properties between the fillers aligned direction and the perpendicular direction, because of the preferred formation of the consecutive network of fillers along the aligned direction.[6, 13-16]

Journal of Materials Chemistry C Accepted Manuscript

Several methods have been used to prepare thermally conductive composites with aligned fillers. In an early report, vertically aligned carbon nanotube (CNT) arrays were used for preparation of epoxy composites by in situ injection; here, a striking difference between through-plane thermal conductivity (λ_Z) and in-plane thermal conductivity (λ_X) was reported ($\lambda_Z/\lambda_X \approx$ 2-5).[14] The pre-aligned CNT arrays were synthesized using chemical vapor deposition (CVD), but they exhibited some difficulties for mass production due to the high cost, complicated process, and time required.[17] In another study, Tian et al. described that the in-plane alignment of the graphite nanoplatelets (GNPs) can be achieved during the lateral flow of the polymer matrix melt under an applied pressure.[18] Although this flow-induced alignment of fillers in the composite can be massively conducted, when the melt viscosity of the composites is increased the alignment weakens significantly. Moreover, Lin and co-workers demonstrated the controlled alignment of magnetically responsive hexagonal boron nitride (hBN) in an epoxy composites by an external magnetic field. The resulting composites exhibited a much higher λ_Z than λ_X.[19] The magnetic alignment might be feasible due to the remote control of the filler alignment. However, the magnetic alignment required the filler have magnetic responsibility. The additional surface modification of the fillers and external magnetic field limited the application of this method. All in all, composites with highly orientated fillers are difficult to obtain using these methods, and the fabrication of such composites remains challenging.

A high-potential material that can be used to prepare this highly ordered hierarchical composites is the one-dimensional (1D) nanofibrillated cellulose (NFC)，which is a new, biobased, and highly crystalline nanofiber. NFC-based nanocomposites have attracted increasing attention in anticipation of high strength, high stiffness, biodegradability, lightweight,

Journal of Materials Chemistry C Accepted Manuscript

transparency, and other biobased functions.[20, 21] NFC has a natural tendency to form a continuous network in which the fillers are homogenously embedded and always adjust their basal plane parallel to the surface.[22] To date, multifunctional NFC-based hybrid materials have been manufactured with various layered silicates, such as talc,[22] montmorillonite (MTM),[23, 24] mica,[25, 26] and vermiculite.[25, 27] Typically, the hybrids exhibit extreme mechanical properties along the aligned direction. Additionally, due to the stratified structure, the hybrids can hinder gas diffusion, resulting in tunable oxygen and water barrier and flame-retardant properties.[28, 29]

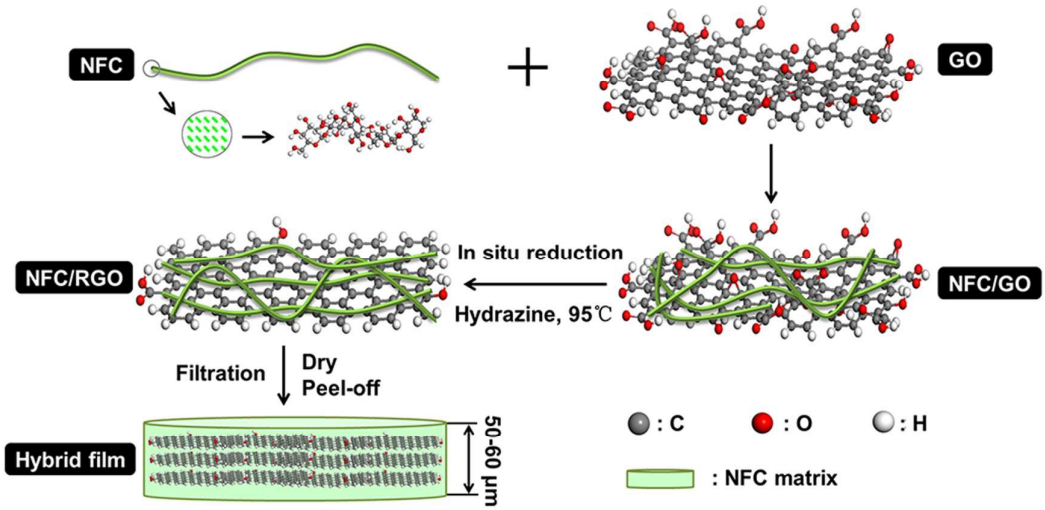

Figure 1. Illustration of the preparation of the hybrid films based on aligned RGO nanosheets and NFC.

In this study, we designed a hybrid film with layered structure based on NFC and RGO nanosheets, which is prepared using in situ reduction and vacuum-assisted self-assembly technique (Figure 1). In this system, NFC not only acts as the matrix in the hybrid films but also plays a role in the stabilization of the RGO in the hybrid dispersion. In the resulting hybrid films, the RGO nanosheets are aligned in the in-plane direction. Large contact areas are achieved between RGO nanosheets, which favor the formation of the consecutive thermally conductive paths, and significantly increase the thermal conductivity in the in-plane direction.

Journal of Materials Chemistry C Accepted Manuscript

Moreover, the thermal conductivity is only well performed along the in-plane direction. The anisotropy of the thermal conductivity is attributed to the different thermal resistance along the in-plane and through-plane directions within the layered hybrid films.

Experimental section

Fabrication of the NFC/RGO Hybrid Films. Graphene oxide (GO) nanosheets were synthesized from natural graphite powder using a modified Hummer's method.[30] The NFC was prepared according to the method reported by Saito (for details, see Supporting Information).[31] The NFC/RGO hybrid films were prepared via in situ reduction and vacuum-filtration process (schematically represented in the Figure S2). A variety of GO dispersions were added in a controlled manner to the NFC suspensions at room temperature and then vigorously stirred for approximately 30 min to yield a homogeneous dispersion with a GO content of 0 to 30 wt% (total solids of 100 mg in 100 mL DI water). 0.2 mL of hydrazine was added into the reaction mixture. The reactants were heated to 95 °C and stirring for 2 h.[32] After cooling to room temperature, the dispersion was vacuum-filtered on a mixed cellulose ester membrane (47 mm in diameter, 0.45 μm pore size). The filter cake was washed with sufficient DI water to eliminate the impurities. The films were dried in vacuum oven at 40 °C overnight before removing the hybrid films from the membranes. The hybrid films that had an NFC/GO weight ratio of 100:0, 95:5, 90:10, 80:20 and 70:30 were named CG0, CG5, CG10, CG20 and CG30, respectively.

For comparison, a two-step approach was also used to fabricate NFC/RGO hybrid films. RGO was first obtained by reducing GO with hydrazine in DI water. Then, the NFC/GO hybrid

Journal of Materials Chemistry C Accepted Manuscript

films were fabricated using the identical method as that in situ reduction approach (for details, see Supporting Information).

Characterization. The Fourier transform infrared (FTIR) spectra were recorded on an Avatar 370 FTIR spectrometer using potassium bromide pellets. The X-ray diffraction (XRD) patterns were collected with a D/MAX2200/PC X-ray diffractometer with Cu Kα radiation (λ = 0.154 nm). Raman spectra were obtained using INVIA confocal micro Raman spectrometer with a 633 nm laser. Thermogravimetric analysis (TGA) was conducted using a T.A. Instruments Q500 Thermo Gravimetric Analyzer under a nitrogen atmosphere at a heating rate of 10 °C•min^{-1}. All of the samples were dried at 40 °C overnight under vacuum before the TGA analysis. Scanning electron microscopy (SEM) images were acquired with a JSM-6700F emission scanning electron microscope. Transmission electron microscopy (TEM) images were acquired using a 200CX 178 transmission electron microscope. The thermal conductivities of the hybrid films were measured using a Netzsch LFA 447 Nanoflash at 25 °C. Each thermal conductivity test was repeated six times, and the values with large errors were excluded. The microscale combustion calorimeter (MCC) tests were conducted on a Govmark MCC-2 Microscale Combustion Calorimeter at a heating rate of 1 °C•s^{-1}. The stress-strain curves were obtained using a Dynamic Thermomechanic Analysis (DMA), from T.A. Instruments (Q800), with a film tension mode. Rectangular strips of 3 × 20 mm with varying thickness were cut from the films and tested at a rate 0.500 N•min^{-1} at room temperature.

Results and discussion

Hydrogen bonding and self-assembly. For the typical preparation, the NFC was dispersed homogeneously in DI water without forming aggregates (Figure 2a) due to the repulsive forces

Journal of Materials Chemistry C Accepted Manuscript

that were generated by the surface carboxyl groups introduced by the NaBr/NaClO/TEMPO oxidation.[33] The diameter of the NFC was 20-50 nm, as determined by TEM (Figure 2b), and had a large aspect ratio, which was important to form a continuous network. The obtained GO nanosheets were uniformly dispersed and were stable in the DI water for more than half a year (Figure 2c). The sheeting morphology of the GO is clearly displayed in the TEM images in Figure 2d. According to the TEM image, GO was fully exfoliated into individual sheets. RGO was synthesized from the reduction of GO using hydrazine in the NFC/GO hybrid dispersion. FTIR, XRD, Raman and TGA analyses showed that GO was reduced to RGO in hybrid films (for the details, see the Supporting Information).

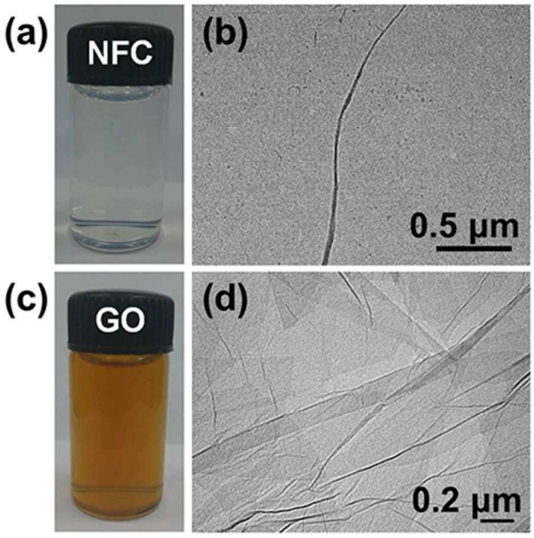

Figure 2. (a) Photograph of NFC suspension. (b) TEM image of NFC. (c) Photograph of GO dispersion. (d) TEM image of GO nanosheets.

Journal of Materials Chemistry C Accepted Manuscript

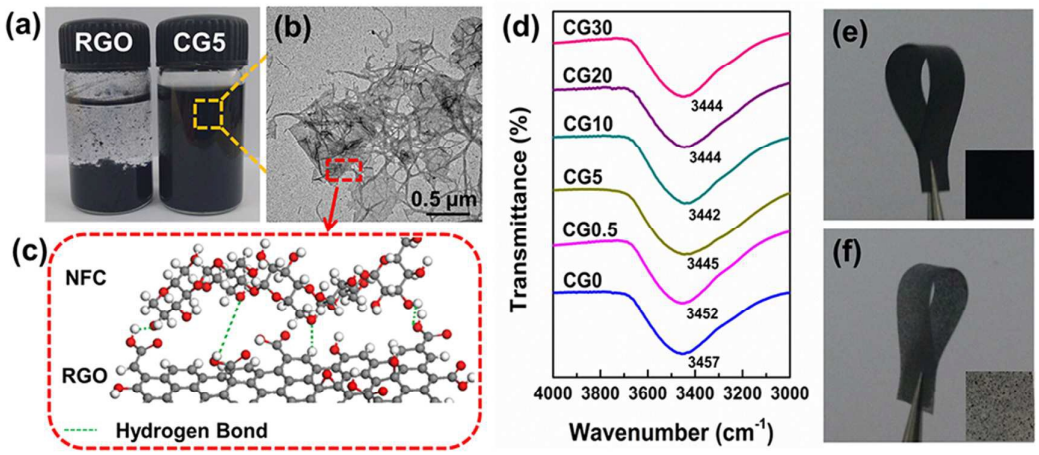

Figure 3. (a) Photographs of RGO (left) and CG5 (right) dispersion. (b) TEM image of the CG5 hybrid dispersion. (c) Schematic of the intermolecular hydrogen bond between NFC and RGO. (d) FTIR spectra of the NFC/RGO hybrid films showing the vibration of –OH groups at wavenumbers 3100-3500 cm^{-1}. (e) Photograph of the hybrid film prepared by in situ reduction and the inset is the detailed representation of the surface. (f) Photograph of the hybrid film prepared by two-step approach and the insert is the detailed representation of the surface.

The reduction of GO in a non-alkali aqueous environment often results in agglomeration of the RGO.[34] Oxygen-containing functional groups that existed on the GO nanosheets, such as carboxyl and hydroxyl groups, cause the GO nanosheets to be highly negatively charged[35] and maintain their stability when dispersed in water. However, most of the oxygen-containing functional groups were removed during the reduction process; thus, the RGO nanosheets exhibited poor stability in DI water (Figure 3a). However, when GO was reduced in the presence of NFC, a uniform and stable dispersion can be obtained. Figure 3a shows the hybrid dispersion containing 5 wt % RGO and 95 wt% NFC, and this hybrid dispersion remained stable for over 3 months. Figure 3b shows that RGO maintained a high aspect ratio after the in situ reduction, and NFC was absorbed on the surface of the RGO nanosheets. The improved dispersity of the RGO

Journal of Materials Chemistry C Accepted Manuscript

could be ascribed to the hydrogen bonding between the hydroxyl segment of the NFC and the residual oxygen-containing groups on the RGO nanosheets (schematically shown in Figure 3c).

Intermolecular hydrogen bonding is one of the most important interactions in polymer composites. There have been reports of strong hydrogen bonds between graphene and highly polar polyalcohols, such as polyvinyl alcohol (PVA), in which the –OH functional groups of PVA played an important role in participating in hydrogen bonding with oxygen-containing groups of graphene.[36, 37] In another report, 3D porous structures of RGO/cellulose composites were prepared in which the hydrogen bonding between the residual oxygen-containing groups on the RGO sheets and the hydroxyl groups of cellulose facilitated the efficient dispersion of the RGO sheets in the cellulose matrix, leading to an improved thermal stability and crystallinity of the cellulose in the composites.[38] The intermolecular hydrogen bonding in composites can be monitored by the broad vibration of the –OH at approximately 3100-3500 cm^{-1}.[36, 39] The presence of hydrogen bonding causes a downshift of the peak. The –OH peaks, shown in Figure 3d, clearly indicate a downshift in the NFC/RGO hybrid films, confirming the hydrogen bonding between the NFC and RGO nanosheets. Therefore, NFC not only constituted the matrix phase of the hybrid films but also acted as a stabilizer for RGO to ensure the stability of the dispersion.

Because of the even distribution of the RGO nanosheets in the hybrid dispersion, the film prepared via the in situ reduction approach is uniform and smooth, as shown in Figure 3e and the inset. However, aggregations of the black graphene nanosheets can be visualized in the film prepared via the two-step approach (Figure 3f and the inset), which may be due to the aggregations of RGO that occurred during the reduction process. Additionally, NFC was

Journal of Materials Chemistry C Accepted Manuscript

incapable of exfoliating the aggregated RGO within the aqueous sample using sonication and agitation. Therefore, unless otherwise mentioned, the NFC/RGO hybrid films were prepared via the in situ reduction approach.

The hybrid films were fabricated via the self-assembly of NFC and RGO under vacuum. The vacuum-assisted self-assembly is advantageous for the rapid and scaling-up of the fabrication of the hybrid films, compared to layer-by-layer (LbL) assemble,[40, 41] freeze casting,[42, 43] and solvent-casting methods.[36, 44] During the filtration, a controlled multi-filtration process (20 mL each time) was used to minimize the disordered layering structure that was caused by the water flow. Under the vacuum pressure, the RGO nanosheets, similar to many layered silicates (e.g., MTM, talc, mica, kaolin), tend to adjust their basal plane parallel to the surface. The alignment appeared to be driven by compressive force generated by the lowering of the air-water interface during solvent removal according to the *Semi-ordered Accumulation* mechanism.[45] This mechanism entails the formation of a loose, semi-ordered aggregate of nanosheets at the filter surface. As excess solvent is removed, and the solvent level contacts the top of the semi-ordered nanosheet mass, a second, compressive phase of paper formation begins. This compression serves to concurrently reduce the spacing between nanosheets while orienting them parallel to the air-water interface, producing a higher degree of order simultaneously throughout the structure. Because of hydrogen bond between the RGO nanosheets and NFC, this alignment can also be extended to NFC/RGO systems. As a result, the well-aligned RGO in the NFC matrix was formed by accumulating nanosheets and nanofibers from the bottom to the top.[22, 23, 46-48] The as-prepared hybrid films were 50-60 μm in thickness. The pure NFC film was

Journal of Materials Chemistry C Accepted Manuscript

transparent; however, the NFC/RGO hybrid films were blackish and translucent or opaque (Figure S6).

Thermal conductivities. The thermal conductivities of the films were measured using a laser flash system. Disks with the diameter of 12.7 mm and 25.0 mm were punched out from the as-prepared films for the λ_Z and λ_X measurements, respectively. The detailed mechanism and methodology of the laser flash system has been reported by Xiang and in our previous study.[49, 50]

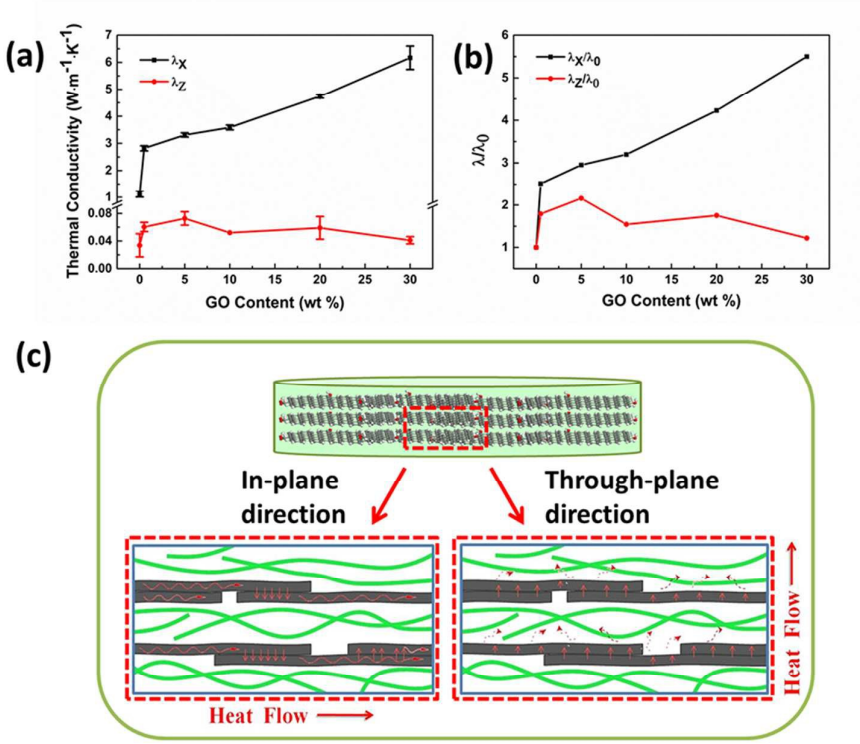

Figure 4. (a) λ_X and λ_Z (b) λ_X/λ_0 and λ_Z/λ_0 of NFC/RGO hybrid films with varied GO content. (c) Schematic diagram of thermal conductivities of hybrid films along in-plane and through-plane directions.

As displayed in Figure 4a, a distinct contrast between the λ_X and λ_Z of the NFC/RGO hybrid films is observed. The value of λ_X greatly surpassed the value of λ_Z. For the in-plane direction, the λ_X increased monotonically with the increase of GO loading and reached 6.168 $W \cdot m^{-1} \cdot K^{-1}$ at 30 wt% GO loading with a 550% thermal conductivity enhancement (TCE)

Journal of Materials Chemistry C Accepted Manuscript

relative to the neat NFC films. For the through-plane direction, the λ_Z varied over the range of 0.034-0.072 $W \cdot m^{-1} \cdot K^{-1}$, which was approximately 1/50 to 1/150 of corresponding λ_X values (1.122-6.168 $W \cdot m^{-1} \cdot K^{-1}$) at the same GO loading. Furthermore, the normalized thermal conductivities (λ/λ_0) indicated that the samples possess a higher thermal conductivity enhancement efficiency along the in-plane direction (Figure 4b). Even when 0.5 wt% of GO was added, a TCE of 151% was obtained, which exhibits a higher efficiency than the polymer-based nanocomposites that contain randomly distributed graphene at a comparable filler content. For example, a 2.0 wt% inclusion of the exfoliated chemically treated graphite platelet and 0.5 wt% of the polymer chains grafted single layer graphene nanosheets increased the thermal conductivity of the epoxy resin and the polystyrene by only 55% and 46%, respectively.[51, 52]

The anisotropy of the thermal conductivity is due to the layered structure that is composed of the aligned RGO nanosheets in the NFC matrix (schematically shown in Figure 4c). The vacuum-assisted self-assembly led to a closely packed and aligned laminated structure in which each basal plane of each RGO nanosheet was nearly parallel to the surface of the films. A large contact area was achieved between the adjacent RGO nanosheets in this structure; therefore, the interface thermal resistance was minimized when heat was transferred along the in-plane direction.[12] With more RGO in parallel along the in-plane direction, the thermal resistance of the heat conduction decreased further. Thus, the graphene–graphene linkages provided direct thermally conductive paths for heat conduction along the plane direction. Consequently, a relatively higher thermal conductivity and enhancement efficiency can be achieved along the in-plane direction. However, in the direction perpendicular to the surface, NFC existed between

Journal of Materials Chemistry C Accepted Manuscript

the RGO layers. Moreover, the λ_Z of the neat NFC (0.034 $W \cdot m^{-1} \cdot K^{-1}$) was significantly lower than that of the graphene nanosheets. The thermally insulating NFC layer hindered the heat flow transport along through-plane direction. Identical to the famous "wooden barrel effect", the λ_Z value was determined by the thermally insulating NFC portion, and the λ_Z value could barely exceed 0.100 $W \cdot m^{-1} \cdot K^{-1}$. In general, the vacuum-assisted self-assembly produced orientated RGO nanosheets in the NFC matrix and produced hybrid films with anisotropic structures, which led to a different thermal resistance along the in-plane and through-plane directions.

The anisotropy of the thermal conductivity was consistent with the observations thus far in which the ordered arrangement of the fillers with high-aspect ratios imparts composites with an anisotropic thermal conductivity. A ratio (λ_X/λ_Z) of approximately 5-10 for epoxy nanocomposites with a 33 vol% loading of carbon nanosheets was reported.[53] Tanimoto et al. studied the effects of the orientation of hBN on the anisotropic thermal diffusivity, and the ratio was approximately 14:1 between the in-plane and through-plane thermal diffusivity.[54] In a recent study, hot-pressed polystyrene/graphene composites with anisotropic thermally conductive properties were reported in which a maximum of λ_X/λ_Z was 13.[15] To determine the anisotropy degree in the thermal conductivity, a parameter called "anisotropy index" (AI) was introduced and defined as follows:

$$\mathrm{AI} = \lambda_A/\lambda_P \quad (1)$$

Where λ_A is the thermal conductivity along the fillers aligned direction, and λ_P is the thermal conductivity along the direction perpendicular to the aligned fillers. Generally, a larger AI suggests improved alignment of the thermally conductive fillers.[18] Table 1 summarizes the anisotropy indexes of a variety of polymer-based composite materials from prior studies. The

Journal of Materials Chemistry C Accepted Manuscript

data illustrate that the anisotropy of the NFC/RGO hybrid films in this study (approximately 150 for the CG30 hybrid films) is very high.[14, 15, 18, 19, 50, 53-59] Thus, the NFC/RGO hybrid films could be particularly useful in applications that require efficient directional thermal transport.

Table 1. Anisotropy indexes in previous literature.

Ref.	Matrix	Filler	AI[a]	Aligned direction[b]	Filler content[c]	Testing method
19	epoxy	hBN	2	2	11 wt%	laser flash
55	epoxy	BN nanosheet	2.5[d]	2	10 vol%	temperature wave analysis (TWA)
14	epoxy	CNT	2-5	2	10-20 vol%	comparative method
18	epoxy	Graphite nanoplatelet	~5	1	11 wt%	steady-state heat flow and comparative technique
53	epoxy	carbon nanosheets	5-10	1	33 vol%	laser flash
15	PS	GO-PPD	13	1	3 wt%	laser flash
56	CNF foam	GO/SEP/BA	~14	1	10 wt%	transient plane source technique
54	sBPDA−PPD PI	hBN	~14[d]	1	50 vol%	TWA
50	PA	GP_{2000}	26	1	5 wt%	laser flash
57	PVA	m-BN	~30	1	50 vol%	laser flash
58	-	multilayer graphene sheets	54	2	100%	laser flash
59	-	exfoliated graphite nanoplatelets	139	1	100%	laser flash
This work	NFC	RGO	150	1	30 wt%	laser flash

[a] The maximum AI in the literature, which was calculated by author based on the reported thermal conductivities.

[b] 1 represented that the fillers aligned along in-plane direction, and 2 represented that the fillers aligned along through-plane direction.

[c] The amount of filler content reported in the literature in the highest anostropy index.

Journal of Materials Chemistry C Accepted Manuscript

[d] In these literatures, only thermal diffusivity (α) were reported. However, on the basis of the formula: $\lambda = \alpha \bullet Cp \bullet \rho$, $A = \lambda_A / \lambda_P = \alpha_A / \alpha_P$.

To shed light on the anisotropy of the thermal conductivities, the structure of hybrid films was further studied using SEM. The lamellar structure was confirmed via SEM images of cross sections of the hybrid films. Figure 5a-d demonstrated the morphology of the fabricated hybrid films in the cross-sectional directions. The graphene nanosheets were evenly distributed in the cross section and were aligned parallel to the surface of the hybrid films. Similar to the brick-and-mortar structure of natural nacre, a closely packed and regular nanoscale layered structure was presented for CG20 and CG30. The layers of the hybrid films exhibit a slightly wavy appearance and inter-penetrate into the neighboring layers. The layered structure is responsible for the different thermal resistances along the in-plane and through-plane directions. This morphology was also observed in nacre-mimicking organic-inorganic composites, such as the polyelectrolyte/clay composite materials prepared by LbL assemble[60] and in NFC/clay hybrids prepared via vacuum filtration.[23, 24] In the cross-sectional SEM images of CG5 (Figure S7), a hierarchical structure can also be observed, accompanied by more nano-fibrous structures of NFC.

Journal of Materials Chemistry C Accepted Manuscript

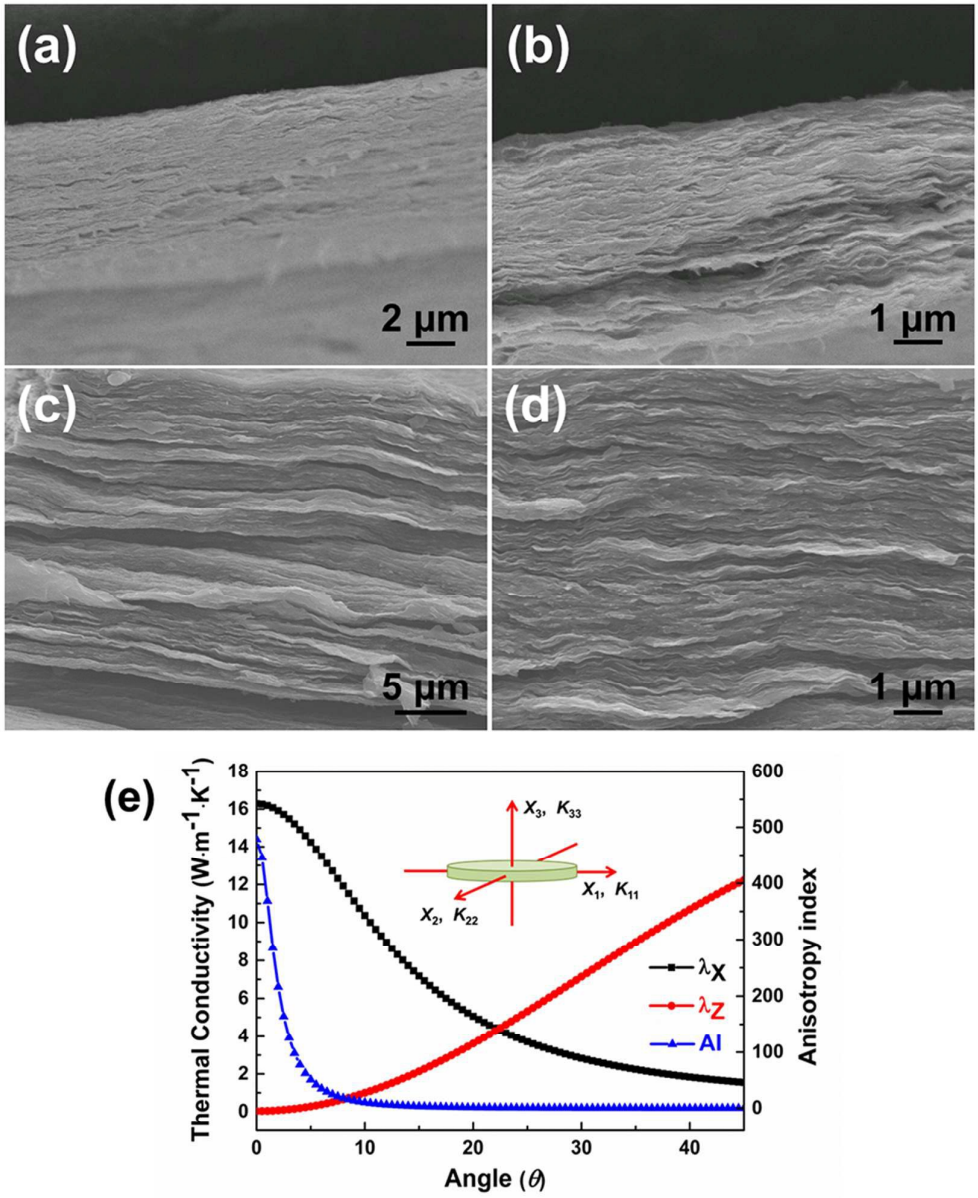

Figure 5. The cross-sectional SEM images of (a, b) CG20, (c, d) CG30. (e) Theoretical AI, λ_X, λ_Z of CG30 hybrid films as function of alignment angle. The insert in (e) is the coordinate axis as well as thermal conductivities along in-plane and through-plane directions used in EMA.

Considering that the layered structure originates from the orientation of the RGO nanosheets, we used the effective medium approximation (EMA) to explore the influence of the graphene orientation on the thermal conductivities and anisotropies of hybrid films. The EMA

Journal of Materials Chemistry C Accepted Manuscript

has been widely used to model the thermal conductivities of polymer composites.[6, 14, 61-63] In this study, the EMA was modified to estimate the in-plane and through-plane thermal conductivities of the NFC/RGO hybrid films under various orientation degrees (for the details, see the Supporting Information). Figure 5e shows the calculated results of CG30 in which the blue, red and black lines represent the theoretical λ_X, λ_Z and AI as a function of θ, respectively. From the curves, it can be conclude that the smaller θ, which signifies an improved orientation of the RGO nanosheets along the in-plane direction, corresponds to a higher AI and a greater disparity between λ_X and λ_Z. This confirms that the aligned graphene in the NFC matrix can produce highly anisotropic thermal conductivities. By comparing the theoretical and experimental data, we observe that the experimental AI, λ_X and λ_Z appeared at $\theta \leq 17$ ° in the curves, which indicates well-aligned graphene. Furthermore, this conclusion was consistent with the morphology of the cross-section surface. Thus, the structure and thermally conductive properties were closely connected by EMA. The RGO nanosheets in the hybrid films aligned along in-plane direction, forming a continuous direct thermal conduction medium along the in-plane direction. However, the graphene-graphene thermally conductive paths were separated by the NFC layer along the through-plane direction.

Journal of Materials Chemistry C Accepted Manuscript

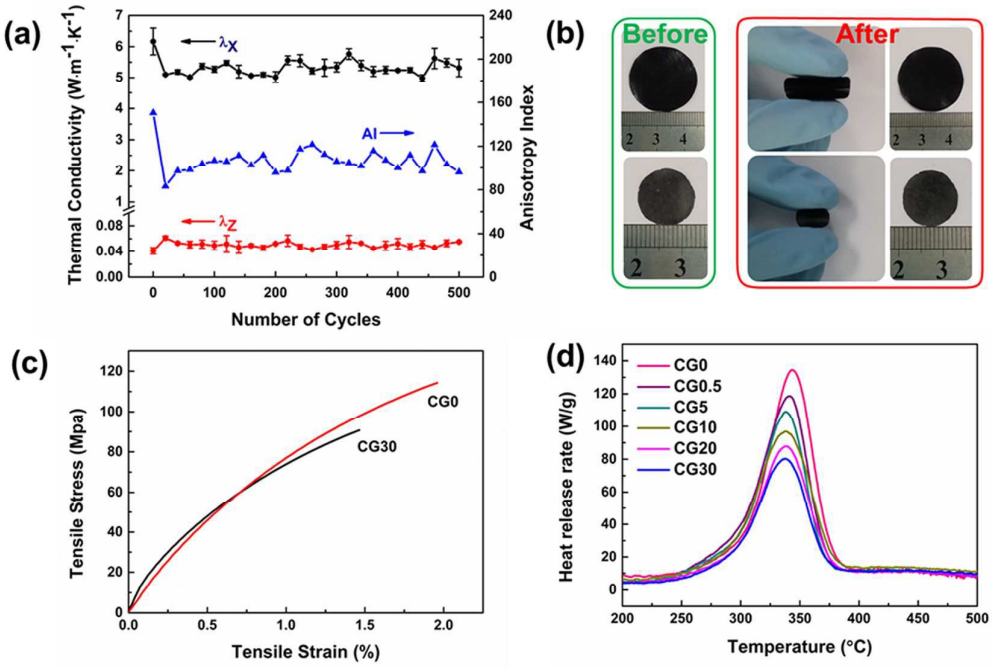

Figure 6. (a) The λ_X, λ_Z and AI of CG30 hybrid film under different numbers of bend cycles. (b)Images of the disks for λ_X, and λ_Z measurements before and after 500 times of mechanical bending. (c) Stress-strain curves of CGO and CG30 hybrid film. (d)HRR curves of NFC/RGO hybrid films with different GO loadings.

Mechanical properties. A highly anisotropic thermally conductive property was achieved in the CG30 hybrid film (λ_X increased to 6.168 $W•m^{-1}•K^{-1}$, λ_Z was only 0.041 $W•m^{-1}•K^{-1}$, the anisotropy index was 150), which was due to the layered structure within the hybrid films. The mechanical property could be another important performance for their applications in thermal management. To evaluate the flexibility of the CG30 film, mechanical stability, which is often used to characterize the flexibility of conductive films,[64, 65] was evaluated using 12.7 mm and 25.0 mm diameter disks for the λ_X and λ_Z measurement. The data were collected every 10 bends which were shown in Figure 6a. The films that suffered from no bending cycles exhibited the most desirable results (the highest AI and λ_X; the lowest λ_Z), which are attributed to the best alignment of the RGO nanosheets. While the λ_X and λ_Z exhibited slight fluctuation during the

Journal of Materials Chemistry C Accepted Manuscript

bending cycles, they varied over the small range of ± 1 to ± 0.018 $W \cdot m^{-1} \cdot K^{-1}$, respectively. Similarly, the AI was also relatively stable. Regarding the EMA results, a $\theta \leq 21$ ° was maintained during the entire bending test, which indicates a good resistance to bending for the layered structure. Besides, after bending 500 times, the disks maintained their shape completely (Figure 6b). The outstanding flexibility is likely due to the combined effect of the intrinsic flexibility of the NFC and the RGO nanosheet and the hydrogen bonding between them. The slight fluctuation during further bend cycles illustrated that the destruction and reconstruction of the structure occurred simultaneously.

Figure 6c shows the stress-strain curves of CG0 and CG30. Note that pure graphene papers that are composed of graphene-graphene linkages exhibited low tensile strength and a porous structure. Regardless, the tensile strength of CG30 was up to 90 MPa, which is slightly lower than that of CG0 (117 MPa). This indicated that the CG30 hybrid films inherited the tensile strength of the NFC. Thus, in the layered hybrid films, NFC acted as an adhesive to provide tensile strength.

Thermal degradation properties. Composites that contain oriented layered fillers often have excellent flame-retardant properties.[46, 66, 67] The thermal degradation properties of NFC/RGO hybrid films were determined using microcombustion calorimetry (MCC) analysis, which is one of the most effective methods to investigate the combustion of materials on a small scale.[68, 69] The experiment consists of first pyrolyzing the sample under a nitrogen atmosphere at a heating rate of 1 $°C \cdot s^{-1}$ from 90 to 750 °C and then pushing the pyrolysis products into a 900 °C combustion furnace, where they are mixed with oxygen. The heat release is calculated based on the combustion process of the pyrolysis products.[66] The typical heat release rate curves for

Journal of Materials Chemistry C Accepted Manuscript

the NFC/RGO hybrid films are provided in Figure 6d, and the corresponding parameters are shown in Table 2. With the incorporation of RGO, the peak heat release rate (PHRR) significantly decreased. For example, when only 0.5 wt% of GO was added, the PHRR decreased by 12.7% (17 W/g) compared with CG0. The total heat release (THR) also exhibits a slight decrease. The presence of RGO nanosheets was responsible for delaying the thermal degradation and enhancing the thermal stability. This phenomenon may be due to the formation of the aligned graphene layer, which can lower the gaseous diffusion. Previous literatures reported that the in-plane orientation of clay resulted in a superior barrier function and a very low through-plane thermal conductivity such that the NFC matrix degradation was delayed.[23, 29] Qian et al. also reported that the high thermal conduction increases the thermal degradation rate of the composites, while the shielding effect of the RGO could decelerate the mass loss during the pyrolysis.[67] In this study, the RGO nanosheets are oriented along the in-plane direction, and the barrier function may significantly improve, while the higher in-plane thermal conductivities accelerate the thermal degradation. However, the PHRR decreased monotonically with the increase of the filler content, indicating that the barrier function was the major reason for the delay in the thermal degradation. Thus, graphene nanosheets were highly aligned in the hybrid films, and they decelerated the escape of volatile products that were generated due to the degradation of NFC, resulting in a delay in the degradation of the hybrid films.

Journal of Materials Chemistry C Accepted Manuscript

Table 2. The MCC data of the NFC/RGO hybrid films with different GO loadings

Sample	GO content (wt%)	PHRR ($W \cdot g^{-1}$)	Decrease of PHRR [a] (%)	THR ($kJ \cdot g^{-1}$)
CGO	0	134	-	6.7
CG0.5	0.5	117	12.7	6.5
CG5	5	109	18.7	5.7
CG10	10	95	29.1	5.6
CG20	20	87	35.1	4.8
CG30	30	80	40.3	4.3

[a] The decrease of PHRR compared with CG0.

As we discussed above, the thermal conductivity of NFC/RGO hybrid films was only well performed in the lateral direction. The highly anisotropic thermally conductive properties of these films can be useful for applications in thermal management. To the best of our knowledge, nowadays, thermal management of modern electronics requires thin films with highly anisotropic thermal conductivity, where the λ_X is substantially larger than the λ_Z.[70, 71] The function of the NFC/RGO hybrid films is to conduct heat away from the hot spots in the in-plane direction while protecting electronic components underneath them from being heated by the adjacent hot spots. Thus, the anisotropic thermally conductive flexible hybrid films have vast potential for applications in various commercial portable electronics such as smart phones, touch panels, and LED lamps with more condensedly packed integrated circuits.[72, 73]

Conclusion

In conclusion, we demonstrated the anisotropic thermally conductive NFC/RGO hybrid films with a laminated structure that were fabricated via a simple in situ reduction and vacuum-assisted self-assembly technique. GO was reduced using hydrazine in the presence of

Journal of Materials Chemistry C Accepted Manuscript

NFC, and a highly stable NFC/RGO hybrid dispersion was achieved because of the hydrogen bonding between the two components. The thermal conductivity of prepared film could be easily reach 6.168 $W•m^{-1}•K^{-1}$, which was 550% enhancement relative to the neat NFC films. Noteworthy, the thermal conductivities were only well performed in the in-plane direction - the through-plane thermal conductivities fluctuate from 0.034 to 0.072 $W•m^{-1}•K^{-1}$. The anisotropy index of the thermal conductivities was as high as 150. The high anisotropy of the thermal conductivity was verified to be due to the high alignment of the RGO nanosheets in the NFC matrix. Accompanied by the anisotropic thermal conductivities was excellent flexibility in terms of stable thermal conductivity over 500 times of mechanical bending cycles. Additionally, the aligned RGO nanosheets significantly delayed the thermal degradation of the hybrid films. This study provides a broad concept for the use of graphene as a superior thermal conductive filler and clarifies that structure-control is an efficient method to regulate the composite properties.

Acknowledgements

This work was financially supported by the National Natural Science Foundation of China (no. 51303101). The authors thank Prof. Yuliang Chu and Prof. Weijun Yu for help with the SEM and TEM measurement

References

1 A. A. Balandin, S. Ghosh, W. Bao, I. Calizo, D. Teweldebrhan, F. Miao and C. N. Lau, *Nano Lett.*, 2008, **8**, 902-907.

2 X. Huang, X. Qi, F. Boey and H. Zhang, *Chemical Society reviews*, 2012, **41**, 666-686.

3 M. Terrones, O. Martín, M. González, J. Pozuelo, B. Serrano, J. C. Cabanelas, S. M. Vega-Díaz and J. Baselga, *Advanced Materials*, 2011, **23**, 5302-5310.

Journal of Materials Chemistry C Accepted Manuscript

4 W. Park, J. Hu, L. A. Jauregui, X. Ruan and Y. P. Chen, *Appl. Phys. Lett.*, 2014, **104**, 113101-11304.

5 M. C. Hsiao, C. C. Ma, J. C. Chiang, K. K. Ho, T. Y. Chou, X. Xie, C. H. Tsai, L. H. Chang and C. K. Hsieh, *Nanoscale*, 2013, **5**, 5863-5871.

6 Q. Li, Y. Guo, W. Li, S. Qiu, C. Zhu, X. Wei, M. Chen, C. Liu, S. Liao, Y. Gong, A. K. Mishra and L. Liu, *Chemistry of Materials*, 2014, **26**, 4459-4465.

7 L. Tian, P. Anilkumar, L. Cao, C. Y. Kong, M. J. Meziani, H. Qian, L. M. Veca, T. J. Thorne, K. N. Tackett and T. Edwards, *ACS nano*, 2011, **5**, 3052-3058.

8 S. Chatterjee, J. W. Wang, W. S. Kuo, N. H. Tai, C. Salzmann, W. L. Li, R. Hollertz, F. A. Nüesch and B. T. T. Chu, *Chemical Physics Letters*, 2012, **531**, 6-10.

9 S. Y. Kim, Y. J. Noh and J. Yu, *Composites Part A: Applied Science and Manufacturing*, 2015, **69**, 219-225.

10 P. Ding, S. Su, N. Song, S. Tang, Y. Liu and L. Shi, *Carbon*, 2014, **66**, 576-584.

11 Z. Tang, H. Kang, Z. Shen, B. Guo, L. Zhang and D. Jia, *Macromolecules*, 2012, **45**, 3444-3451.

12 H. L. Zhu, Y. Y. Li, Z. Q. Fang, J. J. Xu, F. Y. Cao, J. Y. Wan, C. Preston, B. Yang and L. B. Hu, *Acs Nano*, 2014, **8**, 3606-3613.

13 N. Yousefi, X. Lin, Q. Zheng, X. Shen, J. R. Pothnis, J. Jia, E. Zussman and J.-K. Kim, *Carbon*, 2013, **59**, 406-417.

14 A. M. Marconnett, N. Yamamoto, M. A. Panzer, B. L. Wardle and K. E. Goodson, *Acs Nano*, 2011, **5**, 4818-4825.

15 P. Ding, J. Zhang, N. Song, S. Tang, Y. Liu and L. Shi, *Composites Science and Technology*, 2015, **109**, 25-31.

Journal of Materials Chemistry C Accepted Manuscript

16 Z. Wang, X. Shen, M. Akbari Garakani, X. Lin, Y. Wu, X. Liu, X. Sun and J. K. Kim, *ACS applied materials & interfaces*, 2015, **7**, 5538-5549.

17 H. Dai, J. Kong, C. Zhou, N. Franklin, T. Tombler, A. Cassell, S. Fan and M. Chapline, *The Journal of Physical Chemistry B*, 1999, **103**, 11246-11255.

18 X. Tian, M. E. Itkis, E. B. Bekyarova and R. C. Haddon, *Scientific Reports*, 2013, **3**.

19 Z. Y. Lin, Y. Liu, S. Raghavan, K. S. Moon, S. K. Sitaraman and C. P. Wong, *ACS applied materials & interfaces*, 2013, **5**, 7633-7640.

20 I. Siró and D. Plackett, *Cellulose*, 2010, **17**, 459-494.

21 Z. Shi, G. O. Phillips and G. Yang, *Nanoscale*, 2013, **5**, 3194-3201.

22 H. Liimatainen, N. Ezekiel, R. Sliz, K. Ohenoja, J. A. Sirvio, L. Berglund, O. Hormi and J. Niinimaki, *ACS applied materials & interfaces*, 2013, **5**, 13412-13418.

23 A. Liu, A. Walther, O. Ikkala, L. Belova and L. A. Berglund, *Biomacromolecules*, 2011, **12**, 633-641.

24 C. N. Wu, T. Saito, S. Fujisawa, H. Fukuzumi and A. Isogai, *Biomacromolecules*, 2012, **13**, 1927-1932.

25 T. T. Ho, T. Zimmermann, S. Ohr and W. R. Caseri, *ACS applied materials & interfaces*, 2012, **4**, 4832-4840.

26 T. Ho, Y. Ko, T. Zimmermann, T. Geiger and W. Caseri, *Journal of Materials Science*, 2012, **47**, 4370-4382.

27 T. Ho, T. Thu, T. Zimmermann, W. R. Caseri and P. Smith, *Journal of Polymer Science Part B: Polymer Physics*, 2013, **51**, 638-648.

28 C. Aulin, G. Salazar-Alvarez and T. Lindstrom, *Nanoscale*, 2012, **4**, 6622-6628.

Journal of Materials Chemistry C Accepted Manuscript

29 F. Carosio, J. Kochumalayil, F. Cuttica, G. Camino and L. Berglund, *ACS applied materials & interfaces*, 2015, **7**, 5847-5856.

30 H. J. William S. and O. Richard E., *Journal of the Americal Chemical Society*, 1958, **80**, 1339-1339.

31 T. Saito, Y. Nishiyama, J. L. Putaux, M. Vignon and A. Isogai, *Biomacromolecules*, 2006, **7**, 1687-1691.

32 N. D. Luong, N. Pahimanolis, U. Hippi, J. T. Korhonen, J. Ruokolainen, L.-S. Johansson, J.-D. Nam and J. Seppälä, *Journal of Materials Chemistry*, 2011, **21**, 13991-13998.

33 A. Isogai, T. Saito and H. Fukuzumi, *Nanoscale*, 2011, **3**, 71-85.

34 S. Pei and H.-M. Cheng, *Carbon*, 2012, **50**, 3210-3228.

35 C. Wu, X. Huang, X. Wu, L. Xie, K. Yang and P. Jiang, *Nanoscale*, 2013, **5**, 3847-3855.

36 C. Bao, Y. Guo, L. Song and Y. Hu, *Journal of Materials Chemistry*, 2011, **21**, 13942-13950.

37 X. Yang, L. Li, S. Shang and X.-m. Tao, *Polymer*, 2010, **51**, 3431-3435.

38 W. Ouyang, J. Sun, J. Memon, C. Wang, J. Geng and Y. Huang, *Carbon*, 2013, **62**, 501-509.

39 Y. Chen, X. Zhang, P. Yu and Y. Ma, *Chem. Commun.*, 2009, 4527-4529.

40 T. Lee, S. H. Min, M. Gu, Y. K. Jung, W. Lee, J. U. Lee, D. G. Seong and B.-S. Kim, *Chemistry of Materials*, 2015, **27**, 3785-3796.

41 P. Podsiadlo, M. Michel, J. Lee, E. Verploegen, N. W. S. Kam, V. Ball, J. Lee, Y. Qi, A. J. Hart, P. T. Hammond and N. A. Kotov, *Nano Lett.*, 2008, **8**, 1762-1770.

42 S. Deville, E. Saiz, R. K. Nalla and A. P. Tomsia, *Science*, 2006, **311**, 515-518.

43 E. Munch, M. E. Launey, D. H. Alsem, E. Saiz, A. P. Tomsia and R. O. Ritchie, *Science*, 2008, **322**, 1516-1520.

Journal of Materials Chemistry C Accepted Manuscript

44 B. Wang, W. Lou, X. Wang and J. Hao, *Journal of Materials Chemistry*, 2012, **22**, 12859-12866.

45 K. W. Putz, O. C. Compton, C. Segar, Z. An, S. T. Nguyen and L. C. Brinson, *Acs Nano*, 2011, **5**, 6601-6609.

46 H. Sehaqui, J. Kochumalayil, A. Liu, T. Zimmermann and L. A. Berglund, *ACS applied materials & interfaces*, 2013, **5**, 7613-7620.

47 X. Lin, X. Shen, Q. Zheng, N. Yousefi, L. Ye, Y.-W. Mai and J.-K. Kim, *ACS nano*, 2012, **6**, 10708-10719.

48 Z. L. Hou, W. L. Song, P. Wang, M. J. Meziani, C. Y. Kong, A. Anderson, H. Maimaiti, G. E. LeCroy, H. Qian and Y. P. Sun, *ACS applied materials & interfaces*, 2014, **6**, 15026-15032.

49 X. Zeng, L. Ye, S. Yu, H. Li, R. Sun, J. Xu and C. P. Wong, *Nanoscale*, 2015, **7**, 6774-6781.

50 N. Song, J. Yang, P. Ding, S. Tang and L. Shi, *Composites Part A: Applied Science and Manufacturing*, 2015, **73**, 232-241.

51 S. Ganguli, A. K. Roy and D. P. Anderson, *Carbon*, 2008, **46**, 806-817.

52 M. Fang, K. Wang, H. Lu, Y. Yang and S. Nutt, *Journal of Materials Chemistry*, 2010, **20**, 1982-1992.

53 L. M. Veca, M. J. Meziani, W. Wang, X. Wang, F. Lu, P. Zhang, Y. Lin, R. Fee, J. W. Connell and Y.-P. Sun, *Advanced Materials*, 2009, **21**, 2088-2092.

54 M. Tanimoto, T. Yamagata, K. Miyata and S. Ando, *ACS applied materials & interfaces*, 2013, **5**, 4374-4382.

55 H.-B. Cho, M. Mitsuhashi, T. Nakayama, S. Tanaka, T. Suzuki, H. Suematsu, W. Jiang, Y. Tokoi, S. W. Lee, Y.-H. Park and K. Niihara, *Materials Chemistry and Physics*, 2013, **139**, 355-359.

Journal of Materials Chemistry C Accepted Manuscript

56 B. Wicklein, A. Kocjan, G. Salazar-Alvarez, F. Carosio, G. Camino, M. Antonietti and L. Bergstrom, *Nature nanotechnology*, 2015, **10**, 277-283.

57 B.-H. Xie, X. Huang and G.-J. Zhang, *Composites Science and Technology*, 2013, **85**, 98-103.

58 Q. Liang, X. Yao, W. Wang, Y. Liu and C. P. Wong, *ACS nano*, 2011, **5**, 2392-2401.

59 J. Xiang and L. T. Drzal, *Carbon*, 2011, **49**, 773-778.

60 Z. Y. Tang, N. A. Kotov, S. Magonov and B. Ozturk, *Nat. Mater.*, 2003, **2**, 413-418.

61 C.-W. Nan, R. Birringer, D. R. Clarke and H. Gleiter, *Journal of Applied Physics*, 1997, **81**, 6692-6699.

62 Z. Fan, F. Gong, S. T. Nguyen and H. M. Duong, *Carbon*, 2015, **81**, 396-404.

63 K. M. Shahil and A. A. Balandin, *Nano Lett*, 2012, **12**, 861-867.

64 J. Chen, H. Bi, S. Sun, Y. Tang, W. Zhao, T. Lin, D. Wan, F. Huang, X. Zhou, X. Xie and M. Jiang, *ACS applied materials & interfaces*, 2013, **5**, 1408-1413.

65 Y.-L. Tai and Z.-G. Yang, *Journal of Materials Chemistry*, 2011, **21**, 5938-5943.

66 A. L. Higginbotham, J. R. Lomeda, A. B. Morgan and J. M. Tour, *ACS applied materials & interfaces*, 2009, **1**, 2256-2261.

67 X. Qian, B. Yu, C. Bao, L. Song, B. Wang, W. Xing, Y. Hu and R. K. K. Yuen, *Journal of Materials Chemistry A*, 2013, **1**, 9827-9836.

68 Y. Gao, J. Wu, Q. Wang, C. A. Wilkie and D. O'Hare, *Journal of Materials Chemistry A*, 2014, **2**, 10996-11016.

69 A. B. Morgan and M. Galaska, *Polymers for Advanced Technologies*, 2008, **19**, 530-546.

70 J. D. Renteria, S. Ramirez, H. Malekpour, B. Alonso, A. Centeno, A. Zurutuza, A. I. Cocemasov, D. L. Nika and A. A. Balandin, *Advanced Functional Materials*, 2015, **25**, 4664-4672.

Journal of Materials Chemistry C Accepted Manuscript

71 R. Prasher, *Proc. IEEE*, 2006, **94**, 1571-1586.

72 Z. Yan, G. Liu, J. M. Khan and A. A. Balandin, *Nature communications*, 2012, **3**, 827.

73 Y. Zhang, H. Han, N. Wang, P. Zhang, Y. Fu, M. Murugesan, M. Edwards, K. Jeppson, S. Volz and J. Liu, *Advanced Functional Materials*, 2015, **25**, 4430-4435.

Journal of Materials Chemistry C Accepted Manuscript